nature electronics

ARTICLES

https://doi.org/10.1038/s41928-020-00479-4

Check for updates

A molecular shift register made using tunable charge patterns in one-dimensional molecular arrays on graphene

Hsin-Zon Tsai[1,2,3], Johannes Lischner[2,4], Arash A. Omrani[2], Franklin Liou[2,3], Andrew S. Aikawa[2,3], Christoph Karrasch[5], Sebastian Wickenburg[2,3], Alexander Riss[2,10], Kyler C. Natividad[2], Jin Chen[2], Won-Woo Choi[2], Kenji Watanabe[6], Takashi Taniguchi[6], Chenliang Su[1], Steven G. Louie[2,3], Alex Zettl[2,3,7], Jiong Lu[2,8,9] and Michael F. Crommie[2,3,7] ✉

The ability to tune the electronic properties of molecular arrays is an important step in the development of molecule-scale electronic devices. However, control over internal device charge distributions by tuning interactions between molecules has proved challenging. Here, we show that gate-tunable charge patterning can occur in one-dimensional molecular arrays on graphene field-effect transistors. One-dimensional molecular arrays are fabricated using an edge-templated self-assembly process that allows organic molecules (F_4TCNQ) to be precisely positioned on graphene devices. The charge configurations of the molecular arrays can be reversibly switched between different collective charge states by tuning the graphene Fermi level via a back-gate electrode. Charge pinning at the ends of the molecular arrays allows the charge state of the entire array to be controlled by adding or removing an edge molecule and changing the total number of molecules in an array between odd and even integers. Charge patterns altered in this way propagate down the array in a cascade effect, allowing the array to function as a charge-based molecular shift register. An extended multi-site Anderson impurity model is used to quantitatively explain this behaviour.

Assembling electronic devices at the molecular scale involves a number of challenging requirements, including atomically precise structural control, scalability, flexible electronic structure and gate tunability. The potential benefits, however, include miniaturization (along with an increase in device density and speed) and the possibility of new modalities arising from interaction effects that occur in ultra-small systems[1–4]. Relevant platforms include atomic-scale defects[5–7], manipulated atoms[8–12] and molecular systems[13–16]. One promising platform exploits hydrogen vacancies on H-Si(100) surfaces and has yielded impressive atomically precise device structures[5]. Organic-molecule-based device elements, on the other hand, have potential for enhanced electronic tunability[17,18] and self-assembly[14,19,20] characteristics due to their flexible chemical synthesis. The behaviour of molecular elements has been explored previously in metallic break junctions[21–23], self-assembled layers on graphene[24–28] and gate-tunable configurations accessible by scanning tunnelling microscope (STM)[29,30]. However, structural control over molecular systems has so far not been sufficient to yield devices able to exploit interaction effects between different molecular elements.

In this Article, we show that heterogeneous charge configurations can be reversibly manipulated in atomically precise one-dimensional (1D) arrays of 2,3,5,6-tetrafluoro-7,7,8,8-tetracyanoquinodimethane (F_4TCNQ) molecules at the surface of graphene field-effect transistors (FETs). Strong Coulomb interactions between adjacent molecules in dense, self-assembled 1D arrays induce regular, alternating charge patterns that are observable via scanning tunnelling spectroscopy (STS). Application of a gate voltage alters the charge configuration of the molecular array by shifting the graphene device Fermi energy (E_F) relative to the energy of the lowest unoccupied molecular orbitals (LUMOs) in the array. Charge pinning at the ends of the molecular arrays allows the charge state of the entire array to be controlled by tip-based manipulation of the array edge molecules. Charge patterns altered in this way propagate down the array in a cascade effect, allowing the array to function as a charge-based molecular shift register. This behaviour is consistent with the predictions of an extended effective Anderson model, thus allowing quantitative modelling of this 1D interacting molecular device.

Structural characterization of self-assembled molecular arrays on a graphene device

Gate-tunable graphene FET devices were fabricated by placing graphene grown by chemical vapour deposition (CVD) on top of hexagonal boron nitride (h-BN) flakes deposited onto SiO_2 layers grown on doped Si wafers[30]. F_4TCNQ molecules were chosen

[1]International Collaborative Laboratory of 2D Materials for Optoelectronic Science & Technology of Ministry of Education, Institute of Microscale Optoelectronics, Shenzhen University, Shenzhen, China. [2]Department of Physics, University of California at Berkeley, Berkeley, CA, USA. [3]Materials Sciences Division, Lawrence Berkeley National Laboratory, Berkeley, CA, USA. [4]Department of Materials, Imperial College London, London, UK. [5]Institut für Mathematische Physik, Technische Universität Braunschweig, Braunschweig, Germany. [6]National Institute for Materials Science, Tsukuba, Japan. [7]Kavli Energy NanoSciences Institute at the University of California at Berkeley, Berkeley, CA, USA. [8]Department of Chemistry, National University of Singapore, Singapore, Singapore. [9]Centre for Advanced 2D Materials, National University of Singapore, Singapore, Singapore. [10]Present address: Physics Department E20, Technical University of Munich, Garching, Germany. ✉e-mail: crommie@berkeley.edu

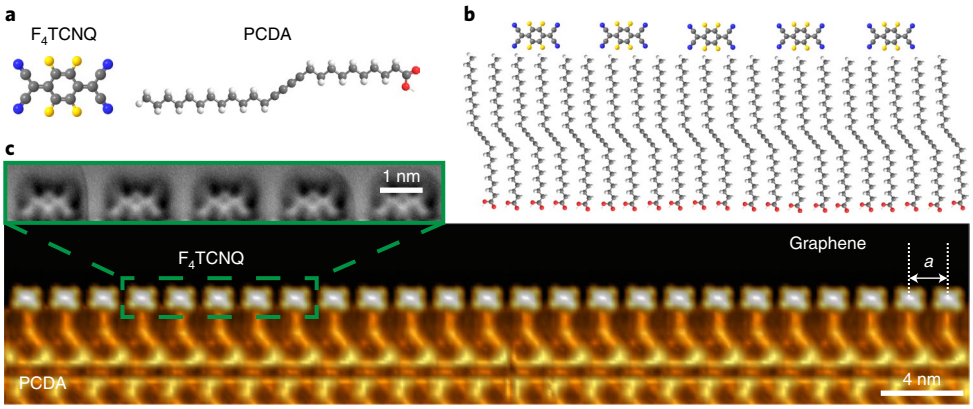

Fig. 1 | Scanned probe images of a 1D F_4TCNQ molecular array. a, Top: sketch of F_4TCNQ and PCDA molecules. Bottom: AFM image showing close-up views of individual F_4TCNQ molecules in a 1D array. **b**, Sketch of a 1D F_4TCNQ molecular array anchored to a PCDA island edge. **c**, Scanning tunnelling microscopy (STM) image of a 50-nm section of an atomically precise 1D F_4TCNQ molecular array anchored to a PCDA island. The periodicity of the molecular array (1.92 nm) corresponds to the moiré lattice constant of the PCDA island on graphene. All STM and AFM images were acquired at $T = 4.5$ K (STM parameters: $V_s = 2$ V, $I_t = 10$ pA, $V_g = 0$ V; AFM parameters: $f_0 = 28.7$ kHz, $Q = 90$ k, $A = 60$ pm, $V_s = 0$ V, $V_g = 0$ V).

as the active molecular elements in this study because they can be reversibly switched between negative and neutral charge states on graphene by application of a back-gate voltage[29] (Fig. 1a). Close-packed linear arrays of F_4TCNQ molecules were formed on graphene FETs through edge-templated self-assembly[31]. This was accomplished by first thermally depositing electronically inert 10,12-pentacosadiynoic acid (PCDA) molecules (Fig. 1a) onto a graphene FET surface to form self-assembled monolayer islands with highly ordered straight edges[32]. These edges were then used to template the growth of thermally deposited F_4TCNQ molecules into 1D arrays, as sketched in Fig. 1b. This process is facilitated by the fact that PCDA islands on graphene form linear moiré patterns that induce periodic stripes along the PCDA island edge (Fig. 1c). F_4TCNQ molecules preferentially adsorb to the PCDA moiré pattern edge maxima[31], leading to the formation of atomically precise molecular arrays with a period of 1.92 nm that can be maintained over large distances around 100 nm (Fig. 1c and Supplementary Fig. 1). Bond-resolved non-contact atomic force microscopy (nc-AFM) images of these molecular arrays show that adjacent molecules are well separated, without significant orbital overlap (Fig. 1c). Molecules within an array, however, are still able to interact with one another via long-range screened Coulomb interactions[33] as well as through the graphene substrate.

Control of molecular charge patterns via a gate voltage

The charge configuration of F_4TCNQ molecular arrays was controlled by changing the FET gate voltage (V_G) and then characterized, molecule by molecule, via STS dI/dV measurements. The results are presented in Fig. 2a, which shows dI/dV spectra of F_4TCNQ molecules in a 16-molecule array held at $V_G = 0$ V (the Fermi level in this case is 0.11 eV below the Dirac point; Supplementary Fig. 3). The spectroscopic peaks identified by the arrows correspond to the F_4TCNQ LUMO states, whereas the sharp feature seen at $V_s = -0.20$ V for each molecule arises due to tip-induced charging[29,34]. Tip-induced charging occurs when the tip acts as a top-gate and causes sufficient band-bending that the LUMO crosses E_F (that is, moves below it) and fills with charge (similar charging behaviour has been seen in STM measurements on isolated F_4TCNQ molecules on graphene FETs[29]). At $V_G = 0$ V, the LUMO orbital of every F_4TCNQ molecule in the array lies above E_F, indicating that the molecules are all in charge-neutral states (that is, the LUMO states are all empty). By contrast, when the gate voltage is raised to $V_G = 60$ V (which causes the Fermi level to rise 0.17 eV above the Dirac point), the LUMO orbitals all fall below E_F and fill with charge (blue shading, Fig. 2c). In this case the molecular array is uniformly filled with charge (one electron per LUMO) and the tip-induced charging peak at $V_s > 0$ now corresponds to emptying a molecule of charge.

The most interesting doping regime is the intermediate regime, $V_G = 30$ V (corresponding to the Fermi level being 0.10 eV above the Dirac point), which moves the LUMO energy level closer to E_F (Fig. 2b). In this regime, the LUMO states (marked by arrows) adopt an unusual electronic structure where they lie alternately above and below E_F for adjacent molecules within the array (charged LUMOs below E_F are shaded blue and neutral LUMOs above E_F are unshaded). Here, the molecular array exhibits an alternating charge pattern where negatively charged molecules sit adjacent to neutral molecules, and their corresponding charging peaks are located on the opposite side of E_F relative to the LUMO energies. This charge alternation behaviour is present only for close-packed molecule chains and is not found in molecule chains where only every other PCDA adsorption site is occupied[31]. We are unable to obtain stable measurements of the LUMO energy for molecules at the ends of the array in this intermediate gating regime, because the STM tip perturbs them too greatly (STS measurements on the end molecules are noisy and depend strongly on the precise position of the STM tip, unlike measurements of the interior molecules, which are stable).

Figure 3a provides a summary plot of the experimental LUMO energies seen in the spectra of Fig. 2a–c for the three different gate voltage levels, along with an STM image of the molecular array. At $V_G = 0$ V the LUMO energies lie solidly in the empty-state regime at 0.1 eV above E_F (corresponding to a uniformly neutral array), whereas for $V_G = 60$ V they fall into the filled-state regime at ~0.18 eV below E_F (corresponding to a uniformly charged array). At $V_G = 30$ V, on the other hand, a periodic bimodal charge pattern is clearly seen where the LUMO energy alternates between +0.1 eV and −0.18 eV for adjacent molecules. This periodic pattern occurs over a relatively narrow range of gate values: $25\text{ V} < V_G < 30\text{ V}$ (corresponding to $0.08\text{ eV} < E_F < 0.10\text{ eV}$ above the Dirac point). Nearby gate voltages that lie outside this range show non-periodic charge alternation patterns, as seen from data obtained at the intermediate gate voltage of $V_G = 20$ V (Supplementary Fig. 4b).

Similar charging behaviour was observed in all 24 of the molecular arrays examined in this study (17 of which were in the 10–20 molecule length range and 7 in the 20–40 molecule length range). Fourteen of the arrays exhibited random defects in their charging patterns in the gate voltage regime where charge alternation occurs. These defects are probably due to electrostatic inhomogeneity arising from factors such as STM tip asymmetry, finite-size effects in

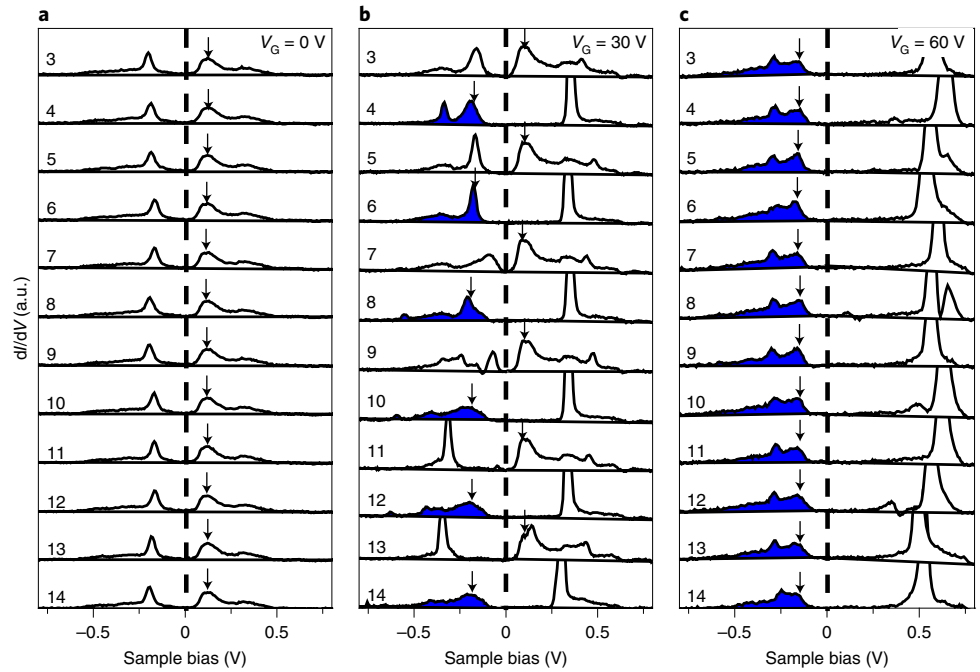

Fig. 2 | Gate-tunable charge patterns in a 1D molecular array. a–c, d*I*/d*V* spectra of 16 F_4TCNQ molecules in a close-packed 1D array at $V_G = 0$ V (**a**), $V_G = 30$ V (**b**) and $V_G = 60$ V (**c**). The integer on the left marks the molecule's location within the array. Arrows indicate the energy position of each molecule's LUMO orbital. Filled-in (blue) peaks signify charged orbitals where the LUMO peak lies below the Fermi level. All experimental data were obtained at $T = 4.5$ K.

the PCDA dielectric islands, as well as charged molecules randomly positioned on the graphene terrace near the molecular arrays. The electronic behaviour of the arrays was not observed to depend significantly on array length.

Theoretical modelling of charge patterns in a 1D Anderson impurity array

We are able to understand the gate-dependent charging behaviour of close-packed 1D F_4TCNQ arrays within the framework of a modified Anderson impurity model. Here, each molecule is described by an impurity state (that is, the LUMO level) and the Hamiltonian of a molecular array consisting of N molecules is given by

$$H = \sum_{i=1}^{N}\left[\sum_{\sigma=\uparrow,\downarrow}\epsilon_L L_{i\sigma}^{+}L_{i\sigma} + Un_{i\uparrow}n_{i\downarrow}\right] + \frac{1}{2}\sum_{i\neq j}W_{ij}n_i n_j + \sum_{sk\sigma}\epsilon_{sk}c_{sk\sigma}^{+}c_{sk\sigma} + H_\Gamma \quad (1)$$

where $n_{i\sigma} = L_{i\sigma}^{+}L_{i\sigma}$ denotes the number of electrons with spin σ in the LUMO level of molecule i and $n_i = n_{i\uparrow} + n_{i\downarrow}$. The orbital energy of the unoccupied LUMO is $\in_L$ and U is the interaction energy between two electrons on the same molecule. Electrons on different molecules interact via the screened potential W_{ij}, where the dominant screening comes from the graphene substrate and is described by a Dirac model dielectric function within the random-phase approximation[35–37]. $c_{sk\sigma}$ removes an electron from the graphene band s with crystal momentum k (measured with respect to the K or K′ points of the graphene Brillouin zone) and energy $\epsilon_{sk} = sv_F k$ (where v_F denotes the Fermi velocity and $s = \pm 1$). H_Γ describes the electron hopping between graphene and F_4TCNQ molecules and is approximated as $H_\Gamma = \Gamma\sum_{i=1}^{N}\sum_{sk\sigma}[L_{i\sigma}^{+}c_{sk\sigma} + \text{h.c.}]$ where Γ is the hybridization energy. Here, $\epsilon_L = -0.1$ eV and $U = 3.1$ eV are obtained from ab initio GW calculations (Supplementary Note 5). Finally, a value for the hybridization energy Γ is required. This quantity depends sensitively on the molecule–graphene separation and the PCDA anchor–F_4TCNQ interaction, and is therefore difficult to determine with first-principles methods. We have chosen $\Gamma = 0.4$ eV (similar to values used in previous work[29]) and verified that our results only depend weakly on this parameter.

To simulate the charging behaviour observed experimentally, we solved the Hartree–Fock equation for each molecule in an array of 16 molecules described by equation (1) and took inter-molecular interactions into account at the mean-field level. As shown in Fig. 3b, we find that the LUMO states in the molecular array are all unoccupied for a Fermi level relative to the Dirac point of $E_F = -0.16$ eV and are all occupied by one electron each when the Fermi level reaches $E_F = +0.15$ eV. At an intermediate Fermi level of $E_F = +0.07$ eV, however, we find that the LUMO occupancies spatially alternate along the molecular array, yielding a periodic charging pattern in Fig. 3b identical to what is seen experimentally in Fig. 3a. The theoretical doping levels here differ slightly from the average experimental values obtained from the gate-dependent Dirac point shift, but are well within the range expected for the doping level inhomogeneity due to the presence of molecules on the surface[38]. Perfect nearest-neighbour charge alternation is only seen over a relatively narrow range of E_F values: $0.06\,\text{eV} < E_F < 0.08\,\text{eV}$. Outside this range, longer-wavelength and non-periodic charging patterns are observed (Supplementary Fig. 4a; no significant length dependence was observed in the charge alternation patterns). This behaviour is similar to the experimental data where periodic nearest-neighbour charge alternation is observed only over a narrow gate voltage range corresponding to $0.08\,\text{eV} < E_F < 0.10\,\text{eV}$. In the experiment, however, we do not observe the longer-wavelength patterns predicted by theory (Supplementary Fig. 4a). This is most likely due to electrostatic inhomogeneity that is present in the experiment but not in the theoretical model.

The observed charge alternation can be interpreted as a nearest-neighbour Coulomb blockade: if an electron occupies a

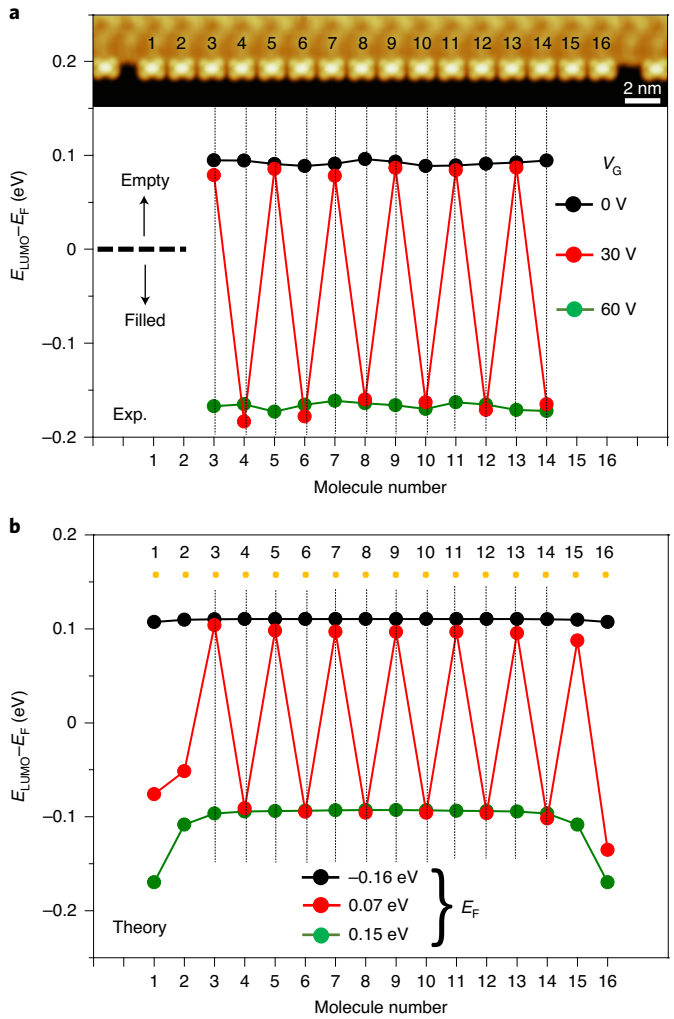

Fig. 3 | Molecular orbital energy in a 1D array. a, Experimental LUMO energies as a function of molecular position for a 1D F_4TCNQ array on graphene (image at top) for gate voltages of 0, 30 and 60 V ($T = 4.5$ K). **b**, Theoretical LUMO energies as a function of molecular position for a simulated array having the same structure as **a** but for different Fermi energy (E_F) values. $E_F < 0$ indicates hole doping and $E_F > 0$ indicates electron doping.

molecule in the array then it is unfavourable for electrons to occupy the two adjacent molecules because the Coulomb potential raises their LUMO energies. The difference in energy between neighbouring LUMO states thus provides a direct measure of the strength of the screened Coulomb interaction between molecules on graphene. Our calculation yields a value of 0.19 eV for this difference, which can be reasonably compared to the measured value of 0.28 eV. The difference between these values is probably due to overestimation of screening in our model, which does not account for the detailed shape of the LUMO orbital (Supplementary Note 5).

Tip-based operation of the shift register

An important result of our model is that the molecules at the two ends of a 1D molecular array are always filled by an electron for the intermediate doping levels that give rise to charge alternation. This is because the ends have only one nearest neighbour and so are subject to less Coulomb repulsion than the interior sites (thus lowering the LUMO energy at the ends). Such end-state charging is accommodated gracefully by arrays with an odd number of molecules, because filled end-states are commensurate with the charge periodicity for odd-number arrays (Supplementary Fig. 5). However, for arrays with an even number of molecules, the charge periodicity is not easily compatible with filled end-states and frustration results. Our model implies that for even-number arrays the charge periodicity will be disturbed at one end by filling the last two molecules with electrons (Fig. 3b), thus yielding a charged dimer defect. The location of the dimer defect (that is, left end versus right end) is chosen in our model by the initial conditions of our calculation (which we solve self-consistently), but for experimental systems we assume the symmetry will be broken by environmental factors (such as nearby defects and so on).

We are unable to directly experimentally test the predicted existence of charged dimer defects for even-number chains due to the fragility of the end-states, which are easily perturbed by the STM tip. However, this predicted odd/even asymmetry has significant experimental consequences for molecular arrays that can be measured, and can lead to new device opportunities. This comes from the fact that if a single molecule is removed from (or added to) the non-defect end of an even-number molecular array, then our model predicts that interior molecules (whose electronic structure is readily accessible experimentally) will all spontaneously switch between neutral and charged states (Supplementary Fig. 5). This, in principle, allows information to be transmitted from one end of a 1D molecular array to the other via a cascade-like mechanism that is equivalent to a charge-based shift register[13,39].

To test this prediction we used tip-based molecular manipulation to remove molecules from one end of an even-number molecular array held at intermediate doping (Fig. 4a) and then characterized the resulting changes in charge state of the interior molecules. We began by removing two molecules from the left end. If this end were to contain the dimer charge defect then we would expect all interior molecules to switch their charge state to accommodate the new charge boundary condition. In the absence of the dimer defect, however, we would expect the interior charge states to all remain unchanged (because then the boundary condition would be unchanged; Supplementary Fig. 5). Figure 4a shows the 16-member molecular array before removing molecules 1 and 2 from the left end. The measured charge states (characterized via STS; Supplementary Fig. 2) are represented by filled circles for negatively charged molecules and open circles for neutral molecules (the end molecules were not measured because of the end-state fragility). Figure 4b shows the same array after removing molecules 1 and 2 by shifting them to the left by one molecular length via tip-based manipulation[40,41]. The charge states of the interior molecules are seen to remain unchanged, indicating that this side did not host a charged dimer defect prior to the manipulation. We then removed one additional molecule from the left end, thus converting the array from an even-number array ($N = 14$) to an odd-number array ($N = 13$). Figure 4c shows the resulting odd-number array and the experimentally measured charge states. The interior molecules are now seen to all exhibit shifted charge states relative to the previous even-number charge configuration (Fig. 4b), a charge reconfiguration that has cascaded throughout the entire array. This behaviour is consistent with the even/odd asymmetry of our theoretical model and verifies charge-based shift-register functionality for atomically precise 1D molecular arrays on graphene.

Conclusions

We have reported a strategy for creating mechanically stable molecular platforms for manipulating information at the nanoscale via applied fields. This is accomplished by using molecular templating to create close-packed 1D molecular arrays whose spatial charge configurations can be tuned by electrostatic gating and tip-based manipulation. This behaviour can be understood through a multi-site Anderson impurity model with screened Coulomb potential that predicts even/odd asymmetry effects arising from charge

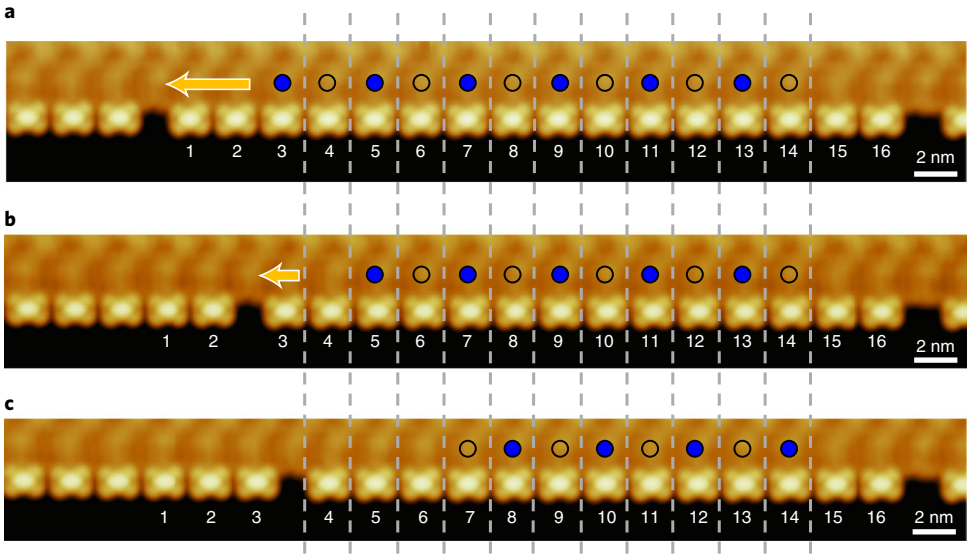

Fig. 4 | 1D array charge pattern control via molecular manipulation. a, STM topography of a 16-molecule F_4TCNQ array. Circles indicate the measured molecular charge state (blue, negatively charged; empty, neutral). **b**, The charge pattern for the same molecular array after removing molecules 1 and 2 on the left end by shifting them one unit to the left with the STM tip (the charge pattern is unchanged compared to **a**). **c**, The charge pattern for the same molecular array after removing molecule 3 on the left by shifting it with the STM tip (the array charge pattern is now seen to be shifted compared to **a** and **b**). Imaging parameters: $V_s = 2$ V, $I_t = 10$ pA, $V_g = 0$ V.

occupancy at the ends of 1D molecular arrays. We have exploited this even/odd end-state asymmetry by using molecular manipulation to create a charge-based molecular shift register. We expect this new technique for controlling molecular charge patterns to be generally applicable to other weakly screened semiconductor systems in addition to graphene. Although STM and STS measurements allow us to understand the principles of operation of our devices, integrating these molecular devices with existing read-out and write-in technologies will require solving a number of difficult challenges such as aligning molecular arrays to macroscopic electrodes and creating molecular structures that have greater temperature stability. The answer to these challenges may well lie within the toolbox of organic synthesis wherein molecules can be designed to self-align and to bind with different functionalized substrates. We expect these concepts to be generalizable to more complex chemically engineered molecular networks that incorporate charge-actuated switching elements.

Methods

Graphene device fabrication. Back-gated graphene/h-BN/SiO_2 devices were prepared by overlaying CVD-grown graphene onto h-BN flakes exfoliated onto a SiO_2/Si substrate. h-BN flakes were exfoliated onto heavily doped silicon wafers and annealed at 500 °C for several hours in air before graphene transfer. The graphene was grown on copper foil via CVD techniques and transferred to the h-BN/SiO_2 substrate via a polymethyl methacrylate stamp[42]. Electrical contact was made to the graphene by depositing Ti (10-nm thick)/Au (30-nm thick) electrodes using a stencil mask.

STM/STS measurements. STM/STS measurements were performed under ultra-high vacuum (UHV) conditions at $T = 5$ K using a commercial Omicron low-temperature STM with tungsten tips. STM topography was obtained in constant-current mode. STM tips were calibrated on a Au(111) surface by measuring the Au(111) Shockley surface state before all STS measurements. STS was performed under open feedback conditions by lock-in detection of the tunnel current driven by a modulation of 6–16 mV (r.m.s.) at 400 Hz added to the tunnelling bias. WSxM software was used to process all STM and AFM images[43].

Data availability

The data that support the findings of this study are available from the corresponding author on reasonable request.

Received: 17 February 2020; Accepted: 1 September 2020;
Published online: 28 September 2020

References

1. Randall, J. N. et al. Digital atomic scale fabrication an inverse Moore's Law—a path to atomically precise manufacturing. *Micro Nano Eng.* **1**, 1–14 (2018).
2. Gehring, P., Thijssen, J. M. & van der Zant, H. S. J. Single-molecule quantum-transport phenomena in break junctions. *Nat. Rev. Phys.* **1**, 381–396 (2019).
3. Aradhya, S. V. & Venkataraman, L. Single-molecule junctions beyond electronic transport. *Nat. Nanotechnol.* **8**, 399–410 (2013).
4. Xiang, D., Wang, X., Jia, C., Lee, T. & Guo, X. Molecular-scale electronics: from concept to function. *Chem. Rev.* **116**, 4318–4440 (2016).
5. Huff, T. et al. Binary atomic silicon logic. *Nat. Electron.* **1**, 636–643 (2018).
6. Achal, R. et al. Lithography for robust and editable atomic-scale silicon devices and memories. *Nat. Commun.* **9**, 2778 (2018).
7. Kalff, F. E. et al. A kilobyte rewritable atomic memory. *Nat. Nanotechnol.* **11**, 926–929 (2016).
8. O'Brien, J. L. et al. Towards the fabrication of phosphorus qubits for a silicon quantum computer. *Phys. Rev. B* **64**, 161401 (2001).
9. Fuechsle, M. et al. A single-atom transistor. *Nat. Nanotechnol.* **7**, 242–246 (2012).
10. Fölsch, S., Martínez-Blanco, J., Yang, J., Kanisawa, K. & Erwin, S. C. Quantum dots with single-atom precision. *Nat. Nanotechnol.* **9**, 505–508 (2014).
11. Khajetoorians, A. A., Wiebe, J., Chilian, B. & Wiesendanger, R. Realizing all-spin-based logic operations atom by atom. *Science* **332**, 1062–1064 (2011).
12. Loth, S., Baumann, S., Lutz, C. P., Eigler, D. M. & Heinrich, A. J. Bistability in atomic-scale antiferromagnets. *Science* **335**, 196–199 (2012).
13. Heinrich, A. J., Lutz, C. P., Gupta, J. A. & Eigler, D. M. Molecule cascades. *Science* **298**, 1381–1387 (2002).
14. Goronzy, D. P. et al. Supramolecular assemblies on surfaces: nanopatterning, functionality and reactivity. *ACS Nano* **12**, 7445–7481 (2018).
15. Steurer, W., Fatayer, S., Gross, L. & Meyer, G. Probe-based measurement of lateral single-electron transfer between individual molecules. *Nat. Commun.* **6**, 8353 (2015).
16. Kocić, N. et al. Implementing functionality in molecular self-assembled monolayers. *Nano Lett.* **19**, 2750–2757 (2019).
17. Xin, N. et al. Concepts in the design and engineering of single-molecule electronic devices. *Nat. Rev. Phys.* **1**, 211–230 (2019).
18. Su, T. A., Neupane, M., Steigerwald, M. L., Venkataraman, L. & Nuckolls, C. Chemical principles of single-molecule electronics. *Nat. Rev. Mater.* **1**, 16002 (2016).

19. Colson, J. W. & Dichtel, W. R. Rationally synthesized two-dimensional polymers. *Nat. Chem.* **5**, 453–465 (2013).
20. Casalini, S., Bortolotti, C. A., Leonardi, F. & Biscarini, F. Self-assembled monolayers in organic electronics. *Chem. Soc. Rev.* **46**, 40–71 (2017).
21. Park, H. et al. Nanomechanical oscillations in a single-C60 transistor. *Nature* **407**, 57–60 (2000).
22. Perrin, M. L. et al. Large tunable image-charge effects in single-molecule junctions. *Nat. Nanotechnol.* **8**, 282–287 (2013).
23. Reed, M. A., Zhou, C., Muller, C. J., Burgin, T. P. & Tour, J. M. Conductance of a molecular junction. *Science* **278**, 252–254 (1997).
24. MacLeod, J. M. & Rosei, F. Molecular self-assembly on graphene. *Small* **10**, 1038–1049 (2014).
25. Järvinen, P. et al. Molecular self-assembly on graphene on SiO_2 and h-BN substrates. *Nano Lett.* **13**, 3199–3204 (2013).
26. Tsai, H.-Z. et al. Molecular self-assembly in a poorly screened environment: F_4TCNQ on graphene/BN. *ACS Nano* **9**, 12168–12173 (2015).
27. Gobbi, M. et al. Periodic potentials in hybrid van der Waals heterostructures formed by supramolecular lattices on graphene. *Nat. Commun.* **8**, 14767 (2017).
28. Phillipson, R. et al. Tunable doping of graphene by using physisorbed self-assembled networks. *Nanoscale* **8**, 20017–20026 (2016).
29. Wickenburg, S. et al. Tuning charge and correlation effects for a single molecule on a graphene device. *Nat. Commun.* **7**, 13553 (2016).
30. Riss, A. et al. Imaging and tuning molecular levels at the surface of a gated graphene device. *ACS Nano* **8**, 5395–5401 (2014).
31. Lu, J. et al. Frustrated supercritical collapse in tunable charge arrays on graphene. *Nat. Commun.* **10**, 477 (2019).
32. Alaboson, J. M. P. et al. Templating sub-10-nm atomic layer deposited oxide nanostructures on graphene via one-dimensional organic self-assembled monolayers. *Nano Lett.* **13**, 5763–5770 (2013).
33. Wong, D. et al. Spatially resolving density-dependent screening around a single charged atom in graphene. *Phys. Rev. B* **95**, 205419 (2017).
34. Brar, V. W. et al. Gate-controlled ionization and screening of cobalt adatoms on a graphene surface. *Nat. Phys.* **7**, 43–47 (2010).
35. Shung, K. W. K. Dielectric function and plasmon structure of stage-1 intercalated graphite. *Phys. Rev. B* **34**, 979–993 (1986).
36. Wunsch, B., Stauber, T., Sols, F. & Guinea, F. Dynamical polarization of graphene at finite doping. *New J. Phys.* **8**, 318–318 (2006).
37. Hwang, E. H. & Das Sarma, S. Dielectric function, screening, and plasmons in two-dimensional graphene. *Phys. Rev. B* **75**, 205418 (2007).
38. Lin, L., Liao, L., Yin, J., Peng, H. & Liu, Z. Building graphene p–n junctions for next-generation photodetection. *Nano Today* **10**, 701–716 (2015).
39. Hopfield, J. J., Onuchic, J. N. & Beratan, D. N. A molecular shift register based on electron transfer. *Science* **241**, 817–820 (1988).
40. Wang, Y. et al. Mapping Dirac quasiparticles near a single Coulomb impurity on graphene. *Nat. Phys.* **8**, 653–657 (2012).
41. Wang, Y. et al. Observing atomic collapse resonances in artificial nuclei on graphene. *Science* **340**, 734–737 (2013).
42. Jung, H. S. et al. Fabrication of gate-tunable graphene devices for scanning tunneling microscopy studies with coulomb impurities. *J. Vis. Exp.* **101**, e52711 (2015).
43. Horcas, I. et al. WSXM: a software for scanning probe microscopy and a tool for nanotechnology. *Rev. Sci. Instrum.* **78**, 013705 (2007).

Acknowledgements

This work was funded by the US Department of Energy, Office of Science, Office of Basic Energy Sciences, Materials Sciences and Engineering Division under contract no. DE-AC02-05-CH11231 (Nanomachine program KC1203; STM imaging and spectroscopy and theory). Work at the Molecular Foundry was supported by the Office of Science, Office of Basic Energy Sciences, of the US Department of Energy under contract no. DE-AC02-05-CH11231 (graphene growth and growth characterization). Device fabrication was supported by National Science Foundation grant no. DMR-1807233. The GW calculations were supported by the National Science Foundation grant no. DMR-1926004. K.W. and T.T. acknowledges support from MEXT Japan grant no. JPMXP0112101001 (characterization of BN crystals) and CREST, JST no. JPMJCR15F3 (growth of BN crystals). A.A.O. acknowledges support from the Swiss National Science Foundation (SNSF) Postdoctoral Research Fellowship under grant no. P2ELP2-151852. J. Lischner acknowledges support from ARCHER UK National Supercomputing Service under EPSRC EP/L000202 and EP/R029431 (simulations). J. Lu acknowledges support from the Singapore Ministry of Education grant no. R-143-000-A06-112 (data analysis). H.-Z.T. acknowledges postdoctoral fellowship support from the Shenzhen Peacock Plan (grant nos. KQJSCX20170727100802505 and KQTD2016053112042971).

Author contributions

H.-Z.T. and J. Lu designed and performed the experiments and analysed the data. J. Lischner performed the theoretical modelling through a multi-site Anderson impurity model. A.A.O., F.L., A.S.A., S.W., C.K., C.S. and A.R. helped with the experiments and gave technical support and conceptual advice. A.Z., K.C.N., J.C. and W.-W.C. facilitated sample fabrication. K.W. and T.T. gave technical support and grew h-BN for the device. S.G.L. supervised the theoretical calculations. M.F.C. supervised the experiments and data analysis. H.-Z.T., J. Lischner, J. Lu and M.F.C. wrote the manuscript.

Competing interests

The authors declare no competing interests.

Additional information

Supplementary information is available for this paper at https://doi.org/10.1038/s41928-020-00479-4.

Correspondence and requests for materials should be addressed to M.F.C.

Reprints and permissions information is available at www.nature.com/reprints.

Publisher's note Springer Nature remains neutral with regard to jurisdictional claims in published maps and institutional affiliations.